

Structural quantum criticality and superconductivity in iron-based superconductor $\text{Ba}(\text{Fe}_{1-x}\text{Co}_x)_2\text{As}_2$

Masahito YOSHIZAWA*¹, Daichi KIMURA^{1,4}, Taiji CHIBA¹, Abdusalam ISMAYIL¹,
Yoshiki NAKANISHI^{1,4}, Kunihiro KIHOU^{2,4}, Chul-Ho LEE^{2,4}, Akira IYO^{2,4},
Hiroshi EISAKI^{2,4}, Masamichi NAKAJIMA^{3,4}, and Shin-ichi UCHIDA^{3,4},

¹ Graduate School of Engineering, Iwate University, Morioka 020-8551, Japan

² National Institute of Advanced Industrial Science and Technology (AIST), Tsukuba 305-8568, Japan

³ Graduate School of Science, The University of Tokyo, Tokyo 113-0033, Japan

⁴ Transformative Research-project on Iron Pnictides (TRIP), Japan Science and Technology Agency, Tokyo 102-0075, Japan

We investigated the elastic properties of the iron-based superconductor $\text{Ba}(\text{Fe}_{1-x}\text{Co}_x)_2\text{As}_2$ with eight Co concentrations. The elastic constant C_{66} shows large elastic softening associated with the structural phase transition. The C_{66} was analyzed base on localized and itinerant pictures of Fe-3d electrons, which shows the strong electron-lattice coupling and a possible mass enhancement in this system. The results resemble those of unconventional superconductors, where the properties of the system are governed by the quantum fluctuations associated with the zero-temperature critical point of the long-range order; namely, the quantum critical point (QCP). In this system, the inverse of C_{66} behaves just like the magnetic susceptibility in the magnetic QCP systems. While the QCPs of these existing superconductors are all ascribed to antiferromagnetism, our systematic studies on the canonical iron-based superconductor $\text{Ba}(\text{Fe}_{1-x}\text{Co}_x)_2\text{As}_2$ have revealed that there is a signature of "structural quantum criticality" in this material, which is so far without precedent. The elastic constant anomaly is suggested to concern with the emergence of superconductivity. These results highlight the strong electron-lattice coupling and effect of the band in this system, thus challenging the prevailing scenarios that focus on the role of the iron 3d-orbitals.

KEYWORDS: iron-based superconductor, elastic constant, quantum criticality, electron-lattice coupling

1. Introduction

Iron-based superconductors have been studied actively worldwide as new high-temperature superconductors. Their superconducting transition temperature is as high as that of cuprates, and superconductivity emerges in the system with the ferromagnetic Fe element.¹⁾ These characteristics are evoking global interest in the mechanism of superconductivity.¹⁾ Among the many iron-based superconductors, $\text{Ba}(\text{Fe}_{1-x}\text{Co}_x)_2\text{As}_2$ is suitable for basic research, because it provides high-quality large single crystals. The crystal structure of the parent compound, BaFe_2As_2 , is shown in Fig. 1(a).²⁾ It has a tetragonal crystal structure at room temperature. This becomes an orthorhombic structure at the structural transition temperature $T_S = 140$ K accompanying the appearance of the long-range antiferromagnetic order²⁾ as shown in Fig. 1(b), which is viewed from the c -axis.³⁾ T_S decreases when Co is substituted for Fe, and superconductivity appears at $x = 0.03$.^{4,5)} T_S falls to zero at $x = 0.07$, where the superconducting temperature T_{sc} becomes highest, reaching 25 K. The magnetic ordering temperature T_N coincides with T_S for $x = 0$, and for samples in which x is less than 0.03, T_N is always lower than T_S . Such a phase diagram showing the coexistence of magnetic order and superconductivity has been observed in the rare-earth compound CePd_2Si_2 and the uranium compound UGe_2 , where superconductivity appears near the quantum critical point (QCP).^{6,7)}

Intensive studies on QCP have led to a new paradigm in physics in which magnetic fluctuation mediates superconductivity. In the case of iron-based superconductors, the mech-

anism of superconductivity has so far been discussed based on the origin of the adjacent magnetic and structural phases, whether magnetic or orbital.^{8,9)} Mazin *et al.* and Kuroki *et al.* predicted that a fully gapped sign-reversing s -wave state (s_{\pm} state) would be realized by magnetic instability.^{10,11)} On the other hand, Kontani and Onari, and Yanagi *et al.* proposed a conventional s -wave state without sign reversal (s_{++} state) mediated by orbital fluctuation.^{12,13)} Investigations on the neighboring order and its fluctuation are important to clarify the superconducting properties of iron-based superconductors.

Our experimental tool, ultrasonic measurements, provides

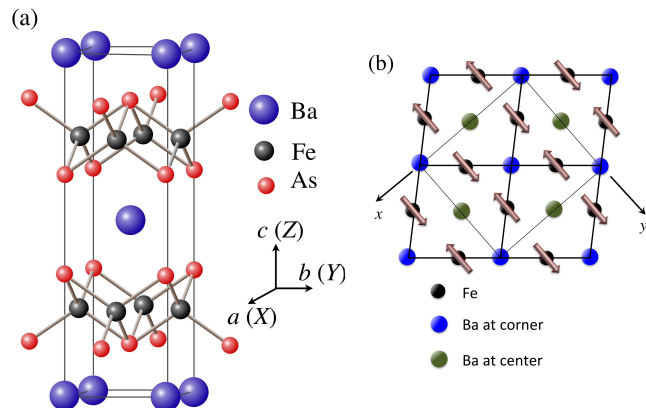


Fig. 1. (Color online) (a) Crystal structure of BaFe_2As_2 , which belongs to the base-centered tetragonal crystal class I_4/mmm , and (b) crystal structure and magnetic order below T_S with the crystal symmetry of $Fmmm$.

*E-mail address: yosizawat@iwate-u.ac.jp

us with information on changes in the symmetry of the lattice system. Strains introduced into the crystal in the elastic constant measurements deform the crystal locally and break the crystal symmetry (symmetry breaking field). When the system encounters either a charge, or orbital (electric quadrupole) order, the elastic stiffness that possesses the same symmetry as, and thus couples with, this order tends to exhibit anomaly (softening in most cases). Accordingly, by examining the temperature (T)-dependence of the anisotropic elastic stiffness C_{ij} , we can obtain fundamental information on the symmetry of the order.

The T -dependence of the elastic stiffness of $\text{Ba}(\text{Fe}_{1-x}\text{Co}_x)_2\text{As}_2$ has been reported for platy samples of BaFe_2As_2 and $\text{Ba}(\text{Fe}_{0.8}\text{Co}_{0.2})_2\text{As}_2$ using the resonant ultrasonic spectroscopy (RUS) method¹⁴⁾ and for a bulk sample of overdoped $\text{Ba}(\text{Fe}_{0.9}\text{Co}_{0.1})_2\text{As}_2$ using pulsed ultrasonic spectroscopy with a phase comparison method.¹⁵⁾ The former study reported a large elastic softening toward T_S in C_{66} , which was present at the percentage ratios of 95% and 18% in BaFe_2As_2 and $\text{Ba}(\text{Fe}_{0.8}\text{Co}_{0.2})_2\text{As}_2$, respectively. The latter study reported that C_{11} , C_{33} , C_{44} , and $\frac{1}{2}(C_{11} - C_{12})$ gradually increased as T decreased, and showed no remarkable anomaly at T_{sc} in contrast with the C_{66} anomaly of 21%.

In the present study, we focused our attention on the huge anomaly in C_{66} and measured the T -dependence of $\text{Ba}(\text{Fe}_{1-x}\text{Co}_x)_2\text{As}_2$ with eight Co concentrations from $x = 0$ to $x = 0.245$ to investigate the neighboring phase and its role in the superconducting properties.

2. Experimental

2.1 Ultrasonic measurements

We measured the elastic constants for $\text{Ba}(\text{Fe}_{1-x}\text{Co}_x)_2\text{As}_2$ using an ultrasonic pulse-echo phase comparison method¹⁶⁾ as a function of temperature from 5 K to 300 K using a cryostat mounted on a Gifford-McMahon (GM) cryocooler. Ultrasound was emitted and detected by LiNbO_3 transducers. X-cut plate of LiNbO_3 at 41° with a thickness of $100 \mu\text{m}$ was used for the transverse waves. The fundamental resonance frequency was 19 MHz. We usually use their higher harmonics of 67 MHz for the experiments. The transducers were glued onto a pair of parallel planes of single crystals using an elastic polymer Thiokol.

Elastic stiffness was obtained by $C = \rho v^2$, where ρ is the density and v is either the longitudinal or transverse sound velocity. The corresponding sound velocities can be obtained by choosing the propagation and displacement directions. Tetragonal crystal symmetry has six independent C_{ij} 's; namely, C_{11} , C_{33} , C_{12} , C_{13} , C_{44} , and C_{66} . The propagation and displacement directions of the sound velocity was $[100]$ and $[010]$ for C_{66} . The sound velocity was obtained by the time interval of the echo train and the sample length, whose accuracy is within a few percent due to the usage of large crystals. The value of ρ was obtained using the data of $x = 0$ and 0.1 .⁴⁾ By assuming Vegard's law, the lattice constant of the $a(b)$ and c axes are $a = b = 0.39636 + 3.8981 \cdot 10^{-4} x$ (nm) and $c = 1.3022 - 0.0421x$ (nm), respectively, for $\text{Ba}(\text{Fe}_{1-x}\text{Co}_x)_2\text{As}_2$. The value of ρ is $6.48 \times 10^3 \text{ kg}\cdot\text{m}^{-3}$ and $6.55 \cdot 10^3 \text{ kg}\cdot\text{m}^{-3}$ for $x = 0$ and 0.245 , respectively. The XYZ coordinate was defined by the unit cell of the $I_{4/mmm}$ crystal structure.²⁾ To prevent damage to the sample due to rapid changes in temperature,

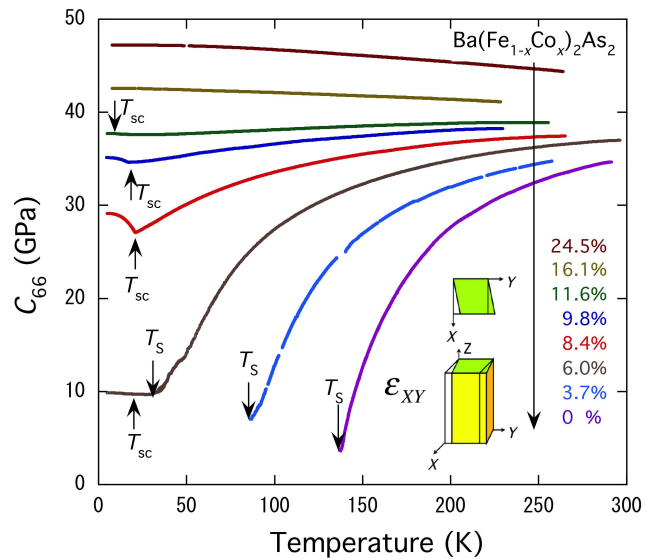


Fig. 2. (Color online) Temperature-dependence of the elastic stiffness C_{66} of $\text{Ba}(\text{Fe}_{1-x}\text{Co}_x)_2\text{As}_2$ with various values.

the rate of change in temperature was carefully controlled so as to be 10 K/h near T_S .³⁾

High-quality large single crystals of $\text{Ba}(\text{Fe}_{1-x}\text{Co}_x)_2\text{As}_2$ used in this work were grown by the self-flux method. Samples with eight Co concentrations $x = 0, 0.037, 0.060, 0.084, 0.098, 0.116, 0.161,$ and 0.245 were prepared. The Co concentration in the grown crystals was determined by energy-dispersive X-ray spectroscopy (EDS) measurement. The Co content of the samples was about 75% of the prepared one. The samples were cut into a rectangular shape, after determining their axis by X-ray Laue photography. The typical size of a sample was $3 \text{ mm} \times 3 \text{ mm}$ in the tetragonal ab (XY) cleavage plane, and 2 mm in thickness on the c (Z)-axis.

2.2 Temperature dependence of C_{66}

Figure 2 shows the T -dependence of C_{66} for samples with $x = 0, 0.037, 0.060, 0.084, 0.098, 0.116, 0.161,$ and 0.245 . C_{66} significantly decreases as T decreases. While a decrease in elastic stiffness is a common feature as a precursor of the structural phase transition, the amount of softening, as much as 80% for $\text{Ba}(\text{Fe}_{0.963}\text{Co}_{0.037})_2\text{As}_2$, is unprecedentedly large. The softening in C_{66} corresponds to the symmetry change from tetragonal to orthorhombic. This is consistent with the structural analysis of this material, where the space group is $I_{4/mmm}$ and F_{mmm} for the high- and low-temperature phases, respectively.²⁾

The decrease in C_{66} with decreasing T is prominent for $x = 0, 0.037,$ and 0.060 , which follow the disappearance of the signal at the structural transition temperature $T_S = 141 \text{ K}$ ($x = 0$), 84.7 K ($x = 0.037$), and 30 K ($x = 0.060$). The data below T_S were not plotted for $x = 0$ and 0.037 , because the sound echo signal disappeared at a certain temperature range below T_S , which may be ascribed to strong scattering of the sound by the orthorhombic domain boundaries. The softening of C_{66} is less prominent as x increases, which is consistent with the disappearance of the structural phase transition. For the superconducting samples, $0.060 \leq x \leq 0.116$, anomalies

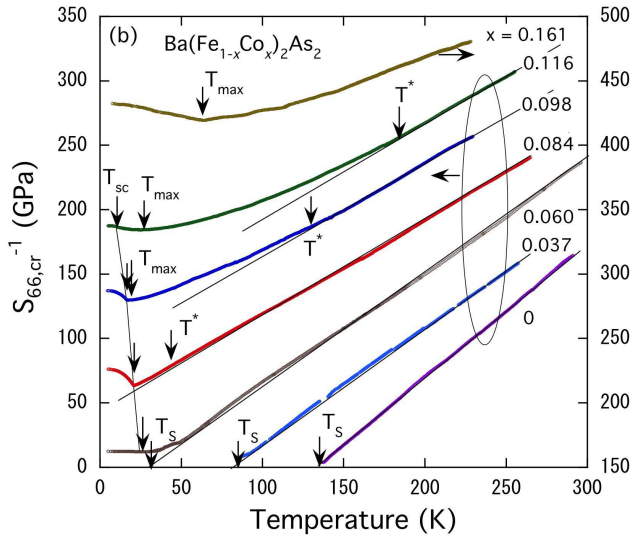


Fig. 3. (Color online) Temperature-dependence of the inverse of $S_{66,cr}$.

are observed at $T_{sc} = 24.0$ K ($x = 0.060$), 20.7 K ($x = 0.084$), 16.5 K ($x = 0.098$), and 10.5 K ($x = 0.116$).

The underdoped samples show a peak at T_{sc} and a step-like anomaly below T_{sc} , as shown in Fig. 8. On the other hand, C_{66} increases below T_{sc} in the overdoped region. This difference will be discussed later. Moreover, the superconducting transition disappears when $x > 0.161$. C_{66} for the samples of $x = 0.161$ and 0.245 shows gradual increases as T decreases, which is a typical behavior for any material, reflecting phonon anharmonicity.

3. Discussion

3.1 Analysis based on localized picture

The observed large elastic anomaly in C_{66} is a precursor of a structural phase transition. Here, we will discuss the origin of the softening in C_{66} from the viewpoint of experimentalists to provide the analysis method.¹⁷⁾ The 3d orbitals are split into E_g doublet and T_{2g} triplet by the electric crystalline field (CEF) in a cubic symmetry. The E_g is split into two singlets, and the T_{2g} is split into one singlet and one doublet by tetragonal CEF of iron-based materials. The remaining doublet can be lifted by the elastic strain, and may cause the elastic anomaly.

We will consider the coupling between the strain ε and an order parameter O as $H = -\lambda O_T \varepsilon_T$. The equivalence of the X and Y axes in tetragonal symmetry leads to the degeneration of the d_{ZX} and d_{YZ} orbitals. This degeneracy is lifted by ε_{XY} or $\varepsilon_{XX} - \varepsilon_{YY}$, and brings about anomalies in the corresponding C_{66} and $\frac{1}{2}(C_{11} - C_{12})$. The strain ε_{XY} can couple with the orbital (quadrupole) O_{XY} . We can calculate the strain susceptibility based on the localized picture of d electron.

$$C_{66} = C_{66,0} - N\lambda^2 \frac{\chi_{66}^0}{1 - I\chi_{66}^0} = C_{66,0} \frac{T - T_C}{T - \Theta} \quad (1)$$

where λ , I , and N are the coupling constant, the intersite interaction, and the number of atoms per unit volume. Here, we adopted the form of $\chi_{66}^0 = \frac{\langle\langle O_{XY}^2 \rangle\rangle}{T}$, for localized d electrons.

Here, we introduce the elastic compliance S_{ij} , which is a component of the inverse C_{ij} matrix. In Eq. (1), the transition undergoes at T_C , where the lattice shows an instability. Elastic compliance represents the structural susceptibility of elastic systems, and corresponds to the magnetic susceptibility χ in magnetic systems. The experimentally observed $S_{66} (= 1/C_{66})$ can be decomposed into the sum of the anomalous contributions that exhibit critical behavior $S_{66,cr}$ and the normal contribution (background) $S_{66,0}$.

$$S_{66} = S_{66}^0 + S_{66,cr} = S_{66,0} \left(1 + \frac{E_{JT}}{T - T_C} \right) \quad (2)$$

where $E_{JT} = T_C - \Theta$. E_{JT} stands for the Jahn-Teller energy, an energy scale that corresponds to the strength of the electron-lattice coupling. Note that this formula has the same form as the Curie-Weiss susceptibility of ferromagnetic materials.

For the analysis, we employed the data on $\text{Ba}(\text{Fe}_{0.755}\text{Co}_{0.245})_2\text{As}_2$ for $S_{66,0}$, and subtract it from the other data. Figure 3 shows the inverse of $S_{66,cr}$ as a function of temperature. It can clearly be seen that $1/S_{66,cr}$ in the underdoped region ($x < 0.070$) exhibits linear T -dependence. This indicates that $S_{66,cr}$ obeys Eq. (2).

In the underdoped samples, T_C in Eq. (2) and T_S obtained by C_{66} are 141 K and 136 K for $x = 0$, 84 K and 81.4 K for $x = 0.037$, and 30 K and 28.2 K for $x = 0.060$, respectively. The closeness of the values in each case suggests the occurrence of ferro-order. This strongly suggests the crystal deformation of ε_{XY} below T_S .

For the underdoped samples, E_{JT} is approximately equal to 50 K. This value is comparable to $\Delta = 20$ K in Ref. [15], which is smaller than our value. The difference between the two experiments is originated from how to choose the background C_0 . While we analyzed the data without a fitting parameter for the background by adopting the data of $\text{Ba}(\text{Fe}_{0.755}\text{Co}_{0.245})_2\text{As}_2$ for C_0 , Goto *et al.* carried out the fitting including the background as adjustable parameters. We performed the analysis by using the same C_0 , which can reveal the systematic behavior though the whole Co concentration. The values of the electron-lattice coupling constant $\lambda \sqrt{\langle\langle O_{XY}^2 \rangle\rangle}$ was calculated from E_{JT} , and is 0.25 eV/Fe for $x = 0.037$.

3.2 Analysis based on band picture

When x exceeds 0.07 , $S_{66,cr}$ deviates from T -linear behavior below a certain temperature T^* ; i.e., 40 K for $x = 0.084$, 130 K for $x = 0.098$, and 190 K for $x = 0.116$. The T -dependence of C_{66} in the overdoped region can be explained by a band picture instead of Eq. (2). Large elastic anomalies compared with iron-based materials have been reported in the A15 superconductor V_3Si and the Laves-phase superconductor CeRu_2 so far.^{18,19)} These anomalies have been ascribed to the large density of states at the Fermi energy. The 3d-orbitals form bands in an iron-based superconductor. The bands located above the Fermi energy at the Γ -point form hole Fermi surfaces and electron pockets at M-points of the zone boundary.¹³⁾ Four M-points (which are identical to X-points in the square lattice formed by Fe atoms) do not become equivalent under ε_{XY} .¹⁷⁾ If a large density of states exists at the M-point, an elastic anomaly may be caused. This provides a natural so-

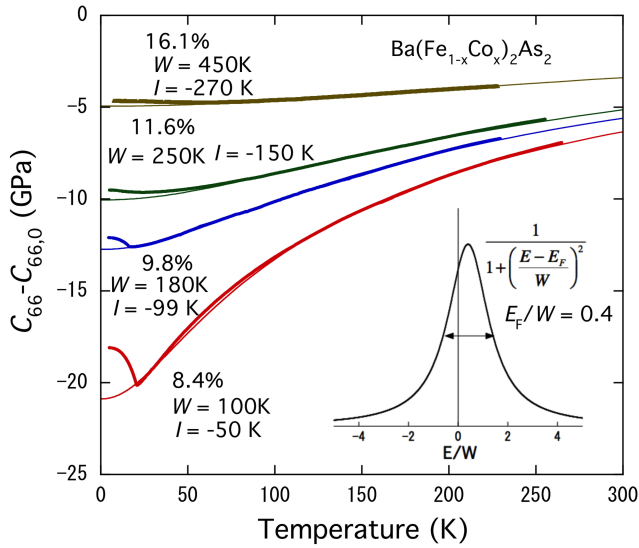


Fig. 4. (Color online) Theoretical fitting of C_{66} by the band Jahn-Teller effect under the assumption of Lorentzian density of states. Adjustable parameters are the bandwidth W and the intersite interaction I .

lution to the question of why the anomaly only emerged in C_{66} .¹⁷⁾ The formula for the elastic constant based on this consideration is as follows:^{20,21)}

$$C = C_0 - (d_{M1} - d_{M2})^2 \frac{\chi_S^0}{1 - I\chi_S^0} \quad (3)$$

$$\chi_S^0 = \frac{1}{k_B T} \sum_k f_k (1 - f_k) = \int dE N(E) f(E)$$

$$N(E) = \frac{N_0}{2} \left[1 + \left(\frac{E - E_F}{W} \right)^2 \right]^{-1}$$

where f is the Fermi-Dirac function, d ($= d_{M1} = -d_{M2}$) is the electron-lattice coupling constant, N_0 is the density of states at Fermi energy E_F , and I is the intersite interaction. The results of fitting by adopting the Lorentzian density of states are shown in Fig. 4.

In this analysis, the main adjustable parameter is the bandwidth W . We fixed $E_F/W = 0.4$ to obtain the best fitting. The value of I is displayed in the figure, depending on the value of x . We added a small constant ranging from 0.8 GPa to 2.45 GPa to the experimental value of C_0 for the fitting. The value of W was 100, 180, 250, and 450 K for the 8.4%, 9.8%, 11.6%, and 16.1% samples, respectively. From the adjustable parameter $N_0 d^2$, the value of d was respectively evaluated as 0.22, 0.25, 0.28, and 0.28 eV/Fe for the four samples, under the assumption that N_0 is approximately equal to $1/W$. The values of N_0 calculated from $N_0 = 1/W$ are respectively 110, 64, 46, and 26 states/eV for the four samples.

The band effect discussed here is called the electronic redistribution mechanism,²²⁾ and is applicable to systems having low resistivity. It is supported experimentally. The resistivity of this system becomes lower in the overdoped region compared with the underdoped region.^{23,24)} Band nesting along the $[\pi/a, \pi/a, 0]$ direction is a characteristic feature of iron-based superconductors. We have no tool for analyzing elastic data based on band nesting. However, we infer that it has

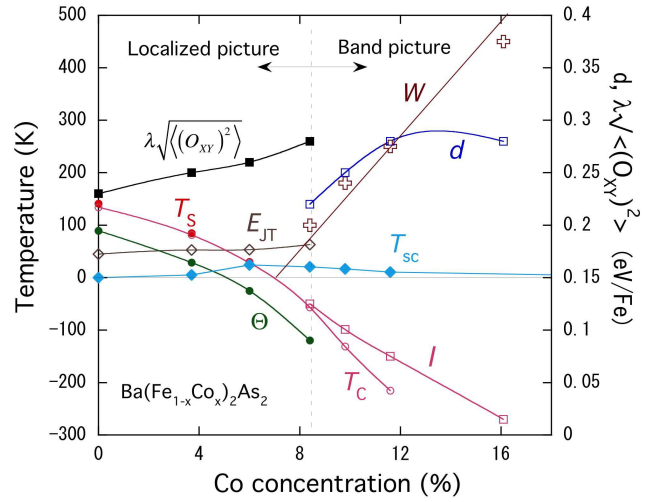


Fig. 5. (Color online) The obtained parameters from the analyses based on the localized and band pictures of Eqs. 2 and 3, respectively. Electron-lattice coupling constants of $\lambda \sqrt{\langle (O_{XY})^2 \rangle}$ was evaluated from E_{JT} . Evaluation method of d is described in the text. The curves are the guides for eyes.

a similar effect to that discussed above, and may cause C_{66} softening. The obtained parameters are summarized in Fig. 5

3.3 Quantum criticality

3.3.1 Phase diagram

Figure 6 summarizes the phase diagram of the $\text{Ba}(\text{Fe}_{1-x}\text{Co}_x)_2\text{As}_2$. The Co concentration-dependence of T_S and T_{sc} are highly consistent with the values reported elsewhere.^{25,26)} We found two characteristic temperatures of T^* and T_{\max} . A possible explanation of T^* is the crossover from the non-Fermi liquid to the Fermi liquid region. The boundary from non-Fermi T -dependence to Fermi liquid T^2 -dependence observed in the resistivity measurements is not clear for $\text{Ba}(\text{Fe}_{1-x}\text{Co}_x)_2\text{As}_2$.²⁷⁾ However, the behavior observed in $\text{BaFe}_2(\text{As}_{1-x}\text{P}_x)_2$ is similar to the case in the present study including the x -dependence of the crossover region.²⁸⁾

We found T_{\max} , which corresponds to the temperature at which $S_{66,cr}$ takes the maximum value ($1/S_{66,cr}$ takes the minimum value), as shown in Figs. 3 and 7. For highly correlated electron systems such as CeCu_2Si_2 , UPd_2Al_3 , and UPt_3 , a similar maximum was reported in the magnetic susceptibility χ , and is interpreted as a Kondo temperature, signaling the coherent motion of f-electrons.²⁹⁾ From this analogy, T_{\max} in this system may suggest the onset of new coherent states.

It would be notable that T^* and T_{\max} go to zero at the QCP concentration of $x_C = 0.07$, indicating the existence of structural QCP at this concentration. In addition, the analysis based on the band picture suggests that the bandwidth W also goes to zero at the same x_C , which suggest a possible mass enhancement toward QCP in this system. Note that this point is located at the center of the superconducting dome. A similar phenomenon was reported for $\text{BaFe}_2(\text{As}_{1-x}\text{P}_x)_2$.³⁰⁾ The obtained phase diagram and various phenomena near the QCP resemble those of the well-known rare-earth compounds and uranium compounds. This coincidence strongly suggests the

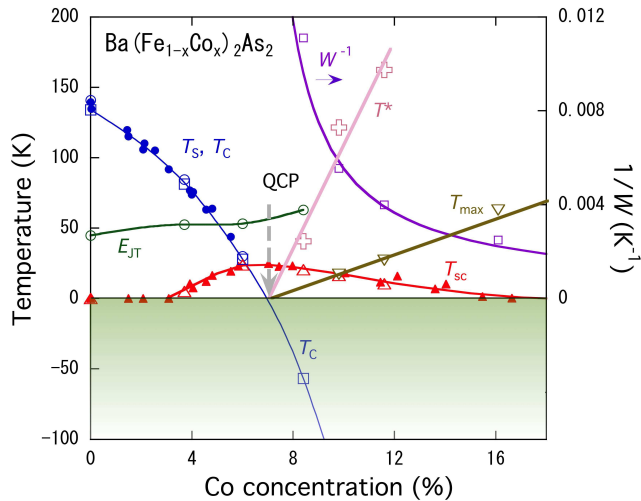


Fig. 6. (Color online) Phase diagram of $\text{Ba}(\text{Fe}_{1-x}\text{Co}_x)_2\text{As}_2$. Filled circles: T_S , and filled triangles: T_C from other studies.^{25,26} Open symbols in this study. The curves are the guides for eyes.

intimate relationship between superconductivity and QCP in this system, similarly to heavy fermion systems where magnetic QCP is believed to be responsible for the emergence of unconventional superconductivity.⁶⁾ The essential difference in this case is that the quantum criticality is associated with structural fluctuations, unlike the magnetic fluctuations in the previous cases. From this reason, we would like to name the structural quantum criticality.

3.3.2 Correlation between elastic anomaly and superconductivity

We now discuss the relationship between the elastic anomaly and superconductivity. As seen in the inset of Fig. 7, the amount of $1/S_{66,cr}$ is proportional to $x - x_C$, where x_C is the QCP concentration of Co; $x_C = 0.07$ for this system. Such behavior is well known in χ of the magnetic QCP. It is surprising that such well-known behavior holds in this system with the respect of S_{66} instead of χ for the magnetic system. As shown in the same figure, T_{sc} decreases with increasing $x - x_C$. So we can recognize an apparent correlation between T_{sc} and $1/S_{66,cr}$ that T_{sc} is a function of $1/S_{66,cr}$. The explanation for this interesting fact is speculated to be as follows. As shown in Fig. 8, the underdoped sample exhibits a small anomaly at T_{sc} , while a large upturn at T_{sc} is seen in the overdoped samples. Once the system enters the orthorhombic phase from the tetragonal phase, structural fluctuations are suppressed in the ordered phase. In the overdoped samples, however, structural fluctuations still survive even at T_{sc} . The amount of the anomaly at T_{sc} correlates with the peak height of $S_{66,cr}$, which is the measure of structural fluctuation. The large anomaly at T_{sc} for the overdoped samples suggests strong coupling between the structural fluctuations and superconductivity. These facts suggest that the origin of $S_{66,cr}$ is deeply related to the emergence of superconductivity.

4. Summary and concluding remarks

The microscopic origin of C_{66} softening has been discussed based on various mechanisms. Large elastic anomalies are often observed in the 4f electron system with a bilinear coupling

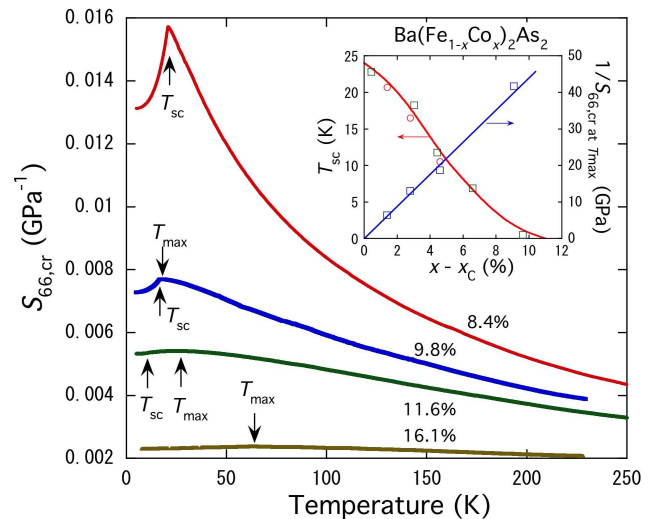


Fig. 7. (Color online) Temperature dependence of $S_{66,cr}$ for the overdoped samples. Inset is T_{sc} from this work and Ref. [25], and the inverse of the peak value of $S_{66,cr}$ as a function of the distance from the QCP concentration $x - x_C$. The curve of T_{sc} is the guide for eyes.

between quadrupole operator O and elastic strain ε with the form of $O\varepsilon$. First, the effect of spin-nematic order has been considered, where the elastic anomaly above T_N is caused by the fluctuation of a pair of magnons at two sublattices.^{14,31)} Spin-nematic order parameter can couple to the strain with a bilinear form. In this case, the nematic order deforms the crystal through the spin-orbit interaction.

On the other hand, theories based on orbital fluctuation have been proposed. Yanagi *et al.* considered Ferro-orbital order accompanying large elastic softening.³²⁾ Kontani *et al.* have discussed a two-orbion process, which is initiated by antiferroquadrupolar fluctuation caused by interband nesting and consisting of a coupling between optical phonon and orbion at the zone-boundary. They showed that two-orbion

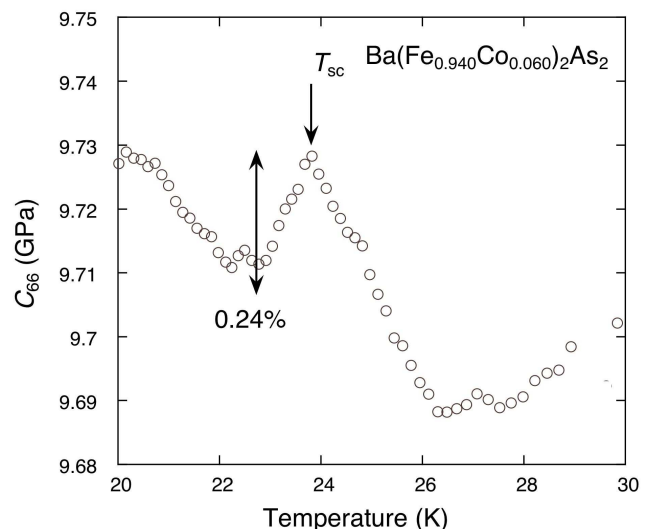


Fig. 8. (Color online) Temperature dependence of C_{66} for the overdoped $\text{Ba}(\text{Fe}_{0.940}\text{Co}_{0.060})_2\text{As}_2$ near T_{sc} in expanded scales

process brings about very large C_{66} softening.³³⁾

As regards the values of the electron-lattice coupling constants λ , the spin-nematic theory and the orbital theory give 17 meV/Fe and 0.2 eV/Fe, respectively.^{14,33)} Our experiment provides the value $\lambda \sim 0.22\text{-}0.25$ eV/Fe for the underdoped samples, and $d \sim 0.2\text{-}0.28$ eV/Fe for the overdoped samples. These values of the coupling constant are considered to be very large, and are consistent with the orbital-based theory both from the localized and band pictures. Generally speaking, a coupling between the magnetic moment and the strain is mediated by a spin-orbit interaction. It is considered that such strong electron-lattice coupling is not caused by weak spin-orbital coupling in transition metals, but by the orbital nature of this system. We suppose that the strong electron-lattice coupling is a characteristic feature of multi-band systems, possessing orbital degrees of freedom. Our results are considered to support the orbital-based theory.

In this article, structural quantum critical behavior was reported for $\text{Ba}(\text{Fe}_{1-x}\text{Co}_x)_2\text{As}_2$. The QCP behavior has been also reported by resistivity measurements and NMR of $\text{Ba}(\text{Fe}_{1-x}\text{Co}_x)_2\text{As}_2$.^{27,34)} The QCP behavior observed in NMR and elastic measurements would be expected to be ascribed to the same origin. Elastic constant is no sensitive probe for magnetism, but sensitive to orbital (quadrupole), contrary to NMR. Our measurement is the observation from the side of orbital (quadrupole).

Further discussions will be necessary on the role of the spin and orbital in the mechanism of superconductivity. However, this system was found to be well characterized by a strong electron-lattice coupling. Therefore, irrespective of whether the spin or orbital mediate superconductivity, the results of the present study suggest that the structural fluctuation must be actively incorporated into their role, and that the orbital degrees of Fe-3d must also be taken into consideration in order to understand the full picture of superconductivity in iron-based compounds.

Acknowledgments

The authors wish to thank H. Fukuyama, H. Hosono, Y. Ōno, H. Kontani, Y. Yanagi, J. Schmalian and Lüthi for their valuable discussions; and M. Nakamura and T. Kowata for their assistance in the experiments. This work was supported by a Grant-in-Aid for Scientific Research on Innovative Areas, gHeavy Electronsh (No. 20102007), of The Ministry of Education, Culture, Sports, Science and Technology, Japan, and the Transformative Research-project on Iron Pnictides of the Japan Science and Technology Agency.

- 1) D. C. Johnston, *Adv. Phys.* 59 (2010) 803.
- 2) M. Rotter, M. Tegel, D. Johrendt, I. Schellenberg, W. Hermes, and R. Pöttgen, *Phys. Rev. B* 78 (2008) 020503(R).
- 3) Q. Huang, Y. Qiu, Wei Bao, M.A. Green, J.W. Lynn, Y.C. Gasparovic, T. Wu, G. Wu and X. H. Chen, *Phys. Rev. Lett.* 101 (2008) 257003.
- 4) A. S. Sefat, R. Jin, M. A. McGuire, B. C. Sales, D. J. Singh and D. Man-

- drus, *Phys. Rev. Lett.* 101 (2008) 117004.
- 5) M. Rotter, M. Tegel and D. Johrendt, *Phys. Rev. Lett.* 101 (2008) 107006.
- 6) N. D. Mathur, F. M. Grosche, S. R. Julian, I. R. Walker, D. M. Freye, R. K. W. Haselwimmer, and G. G. Lonzarich, *Nature* 394 (1998) 39.
- 7) S. S. Saxena, P. Agarwal, K. Ahilan, F. M. Grosche, R. K. W. Haselwimmer, M. J. Steiner, E. Pugh, I. R. Walker, S. R. Julian, P. Monthoux, G. G. Lonzarich, A. Huxley, I. Sheikin, D. Braithwaite and J. Flouquet, *Nature* 406 (2000) 587.
- 8) C. Fang, H. Yao, W. F. Tsai, J-P. Hu, and St. A. Kivelson, *Phys. Rev. B* 77 (2008) 224509.
- 9) F. Krüger, S. Kumar, J. Zaanen, and J. van den Brink, *Phys. Rev. B* 79 (2009) 054504.
- 10) I. I. Mazin, D. J. Singh, M. D. Johannes, and M. H. Du, *Phys. Rev. Lett.* 101 (2008) 057003.
- 11) K. Kuroki, S. Onari, R. Arita, H. Usui, Y. Tanaka, H. Kontani, and H. Aoki, *Phys. Rev. Lett.* 101 (2008) 087004.
- 12) H. Kontani and S. Onari, *Phys. Rev. Lett.* 104 (2010) 157001.
- 13) Y. Yanagi, Y. Yamakawa, and Y. Ōno, *Phys. Rev. B* 81 (2010) 054518.
- 14) R. M. Fernandes, L. H. Van Bebber, S. Bhattacharya, P. Chandra, V. Keppens, D. Mandrus, M. A. McGuire, B. C. Sales, A. S. Sefat, and J. Schmalian, *Phys. Rev. Lett.* 105 (2010) 157003.
- 15) T. Goto, R. Kurihara, K. Araki, K. Mitsumoto, M. Akatsu, Y. Nemoto, S. Tatematsu, and M. Sato, *J. Phys. Soc. Jpn.* 80 (2011) 073702.
- 16) B. Lüthi, *Physical Acoustics in the Solid State*, Springer-Verlag p. 9 (2004).
- 17) M. Yoshizawa, *J. Phys. Soc. Jpn. Online-News and Comments* [July 14, 2011].
- 18) L. R. Testerd, and T. B. Bateman, *Phys. Rev.* 154 (1967) 402.
- 19) T. Suzuki, H. Goshima, S. Sakita, T. Fujita, M. Hedo, Y. Inada, E. Yamamoto, Y. Haga and Y. Ōnuki, *J. Phys. Soc. Jpn.* 65 (1996) 2753.
- 20) P. Thalmeier and B. Lüthi, in *Handbook on the Physics and Chemistry of Rare Earths Vol. 14*, ed. K. A. Gschneidner Jr. and L. Eyring, Amsterdam: Elsevier (1991) p. 245.
- 21) M. Yoshizawa, I. Shirovani, and T. Fujimura, *J. Phys. Soc. Jpn.* 55 (1986) 1196.
- 22) B. Lüthi, *Physical Acoustics in the Solid State*, Springer-Verlag (2004) p. 159.
- 23) F. Rullier-Albenque et al., *Phys. Rev. Lett.* 103 (2009) 057001.
- 24) M. Nakajima, S. Ishida, K. Kihou, Y. Tomioka, T. Ito, Y. Yoshida, C. H. Lee, H. Kito, A. Iyo, H. Eisaki, K. M. Kojima, and S. Uchida, *Phys. Rev. B* 81 (2010) 104528.
- 25) P. C. Canfield, S. L. Bud'ko, Ni Ni, J. Q. Yan, and A. Kracher, *Phys. Rev. B* 80 (2009) 060501(R).
- 26) Y. Laplace, J. Bobroff, F. Rullier-Albenque, D. Colson, and A. Forget, *Phys. Rev. B* 80 (2009) 140501(R).
- 27) N. Doiron-Leyraud, P. Auban-Senzier, S. R. de Cotret, Cl. Bourbonnais, D. Jérôme, K. Bechgaard, and L. Taillefer, *Phys. Rev. B* 80 (2009) 214531.
- 28) S. Kasahara, T. Shibauchi, K. Hashimoto, K. Ikada, S. Tonegawa, R. Okazaki, H. Shishido, H. Ikeda, H. Takeya, K. Hirata, T. Terashima, and Y. Matsuda, *Phys. Rev. B* 81 (2010) 184519.
- 29) Y. Ōnuki, R. Settai, K. Sugiyama, T. Takeuchi, T. C. Kobayashi, Y. Haga, and E. Yamamoto, *J. Phys. Soc. Jpn.* 73 (2004) 769.
- 30) Y. Nakai, T. Iye, S. Kitagawa, K. Ishida, H. Ikeda, S. Kasahara, H. Shishido, T. Shibauchi, Y. Matsuda, and T. Terashima, *Phys. Rev. Lett.* 105 (2010) 107003.
- 31) A. Cano, M. Civelli, I. Eremin, and I. Paul, *Phys. Rev. B* 82 (2010) 020408(R).
- 32) Y. Yanagi, Y. Yamakawa, N. Adachi, and Y. Ōno, *J. Phys. Soc. Jpn.* 79 (2010) 123707.
- 33) H. Kontani, T. Saito, and S. Onari, *Phys. Rev. B* 84 (2011) 024528.
- 34) F. L. Ning, K. Ahilan, T. Imai, A. S. Sefat, M. A. McGuire, B. C. Sales, D. Mandrus, P. Cheng, B. Shen, and H.-H. Wen, *Phys. Rev. Lett.* 104 (2010) 037001.